JOURNAL OF THERMOPHYSICS AND HEAT TRANSFER
Vol. 14, No. 4, October–December 2000

Novel Shadow Image Velocimetry Technique for Inferring Temperature

George Papadopoulos*
Dantec Measurement Technology, Inc., Mahwah, New Jersey 07601

Particle image velocimetry (PIV) methodology is used to robustly determine the velocity of interference patterns caused by variations in the local index of refraction of a time-varying diffusion flame as imaged by simple shadowgraphy. The shadowgraphs are optimized for PIV-based analysis using a novel optical arrangement, and the velocity of the index-of-refraction variants determined from such an acquisition process is shown to correspond primarily to temperature variations within the reacting flow. Integration of this shadowgraph–image–velocity field is subsequently shown to yield the temperature field.

Nomenclature

D = thickness of schliere or flame
L = distance from schliere to photographic screen
n = index of refraction
T = temperature
U = shadow image velocity (SIV) horizontal component
V = SIV vertical component
x = horizontal displacement variable
y = vertical displacement variable
δ = differential
ζ = displacement-correction bias
θ = angular deflection of light beam
κ_0 = shadowgraph configuration-dependent proportionality constant

Introduction

THE use of optical methods for measuring quantities such as velocity, temperature, density, and species in flows has greatly increased our understanding of flow physics, in great part due to the nonintrusive nature of these techniques, which offers a significant advantage over comparable methods. This ability to transparently probe the flow has pushed forward the development of optical methods as viable tools in the basic research, as well as in the applied areas of engineering.

The dependence on a flow system's optical accessibility and response, however, creates difficulties that greatly increase the complexity of optically based measurement methods and thus limit their general applicability. Overcoming such difficulties may not, however, require the invention of totally new approaches but those that merge qualities of existing ones. In certain cases the advantages of separate optical techniques may be combined to create a new technique with improved robustness and certain unique practical possibilities, in the absence of some of the limitations.

The objective of the present paper is to introduce such a novel technique, one that combines classical index-of-refraction-based flow visualization methodology with the acquisition and fast postprocessing of the recently introduced particle image velocimetry (PIV) technique. With this approach, the instantaneous phase displacement information of index-of-refraction gradients that commonly occur in reacting, high-speed flows and variable density flows may be determined.

Received 15 October 1999; presented as Paper 2000-0374 at the AIAA 38th Aerospace Sciences Meeting, Reno, NV, 10–13 January 2000; revision received 26 May 2000; accepted for publication 30 May 2000.

*Applications Engineer, Measurement Consultancy Department, 777 Corporate Drive; george.papadopoulos@dantecmt.com. Senior Member AIAA.

Qualitative information on the local field variations of scalar quantities, such as temperature or density, may be inferred through local index-of-refraction changes by using interferometer-based techniques. The present investigation revolves around flames, but the approach described may be used in other situations where index-of-refraction changes due to field variations are available for visualization. By the use of simple shadowgraphy, the gradients in the local index of refraction of a time-varying diffusion flame were specially imaged and processed at two instants in time using PIV-based image correlation methods to evaluate the instantaneous, whole-field velocity of the interference pattern. Integration of this velocity field was then shown to yield the temperature field.

Background

Visualization Methods

Flames may be visualized using the light deflected by the steep refractive index gradients in flame fronts. The interpretation of the observed patterns of transmitted light is a complex exercise in physical and/or geometric optics. There are three limiting cases: 1) interferometry, where the pattern deflections are proportional to the refractive index n; 2) schlieren photography, which is a dark-field method where the image depends on the first derivative of the refractive index $\mathrm{d}n/\mathrm{d}y$; and 3) shadow photography, where the deflections also depend on the gradient, but because of overlap the images outlined by the caustics are related to the second derivatives of the index of refraction $\mathrm{d}^2n/\mathrm{d}y^2$. These techniques have been reviewed extensively by Weinberg,[1] Weinberg and Wong,[2] and Weinberg[3] and will be described briefly for completeness.

An interference pattern is created by passing a coherent beam through the region of interest and superimposing it with a comparison beam. When properly combined on a screen, the two waves interfere due to phase differences, which produces an image outlining regions of differing optical path length. This can be interpreted quantitatively in terms of density or temperature if the geometry is known.[4] A disadvantage of this technique is that the traveled distance between the image beam and the comparison beam cannot be off by more than a fraction of a wavelength of the light source used to preserve the coherence between the two beams. Thus, extreme care must be practiced to isolate the optical components from structural vibrations.

To cope with the aforementioned hindrance, a single beam system is desirable, and recent applications of point diffraction interferometry (PDI) in combustion hold much promise.[5–8] In a PDI system, both test and reference beams travel along a common path, and a disk consisting of a circular diffraction hole centered in a semi-absorbing thin film, which is placed at the focal point of a decollimating lens, is used to deconvolute the reference beam and to create an interference pattern. This pattern is two dimensional, and the fringes relate directly to the index of refraction. Once properly numbered

and counted, information regarding the density or temperature field may be generated.

Full-field deflection mapping using diagonal parallel grids or Ronchi gratings is sometimes called the moiré effect. Moiré deflectometry was introduced by Kafri,[9] Stricker and Kafri,[10] and Keren et al.[11] as a new noncoherent method for mapping the density field of two-dimensional flow and for making measurement of temperature distributions in flames. Unlike classical interferometry techniques that are generally restricted to the low-noise environment of the laboratory due to their mechanical stability requirements of a fraction of the wavelength, moiré interferometry can be used in more noisy environments because it requires no coherence matching between two separate beams. To a great extent it is a compatible alternative to interferometry. The information provided by moiré deflectometry is the ray deflection map of a light beam passing through or reflected from an object.[9]

In schlieren photography a beam of parallel light from a slit or point source is passed through a region of varying refractive index and brought to a focus on a stop. The stop can be a knife edge, a wire, a small spot, or a grid. Regions containing varying refractive index will be deflected around the stop and can be brought to a focus, which produces an image connecting regions of the same refractive index gradient. The usual schlieren image of a flame locates a surface close to the region of initial temperature change because it measures absolute density gradient rather than fractional change.[1] If a grating is used as a stop, a series of contours is produced that connect regions of equal gradient. This Ronchi grating system is useful for quantitative work. A recent variant of this system, called rainbow schlieren deflectometry, uses a continuously graded color filter as the stop.[12–14] The deflections are converted to variations in color represented by the hue. This latter technique overcomes the problems of nonuniform absorption, diffraction, and shadowgraphy effects prevalent in the conventional schlieren, and it can be used for quantitative measurements.[13,14] Hence, it provides a superior means for determining the temperature and species concentrations that are related to the refractive index distributions the schlieren deflection data provides.

Yet another useful variant of schlieren photography is the focusing schlieren. By the use of a multiple source/stop array, the system can be focused so that it is sensitive to gradients in a single plane. Two separate versions of focusing schlieren were developed. One version, by Kantrowitz and Trimpi,[15] required two well-corrected wide-angle lenses and was limited to a field of view smaller than the lens diameter. The second version, by Burton,[16] required only one lens and could cover a field of view larger than the lens diameter. Attention on this latter schlieren system has recently been rekindled by the introduction of several ideas that eliminated some of the limitations of the technique and reduced the complexity of the system.[17] The ability of the system to focus in a fairly thin portion of the optical path sets it apart from the other line-of-sight techniques and greatly aids in the examination of complex, three-dimensional flows.

The simplest schlieren system is shadow photography. A point source of light, or a small pin-hole with a light focused on to it, is used to generate a divergent or parallel array of beams. Deflections in shadow photography are proportional to the gradient in the refractive index, and a complex pattern results, due to dark regions tending to be in line with the source and schlieren causing them. This is further complicated by the superposition of bright areas of deflected light from other parts of the image.

Weinberg[18] analyzed the deflection of light rays in shadow photography for a flat flame. If L is the distance from the center of the flame to the screen, D is the thickness of the flame, and δy is the height, then for small deflections, as can be seen from Fig. 1,

$$y' = y - \theta L \tag{1}$$

and, because

$$\theta = -\frac{\mathrm{d}n}{\mathrm{d}y} D \tag{2}$$

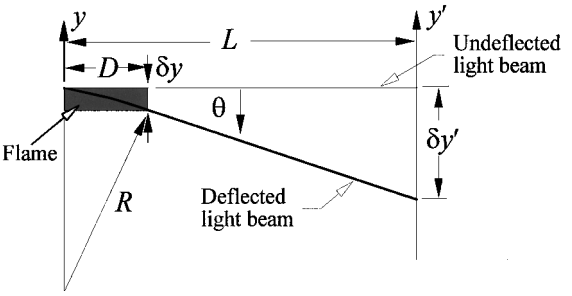

Fig. 1 Light-ray deflection in shadow arrangement using parallel light.

where n is the refractive index, it follows that

$$y' = y + \frac{\mathrm{d}n}{\mathrm{d}y} DL \tag{3}$$

Differentiating yields

$$\delta y' = \delta y + \frac{\mathrm{d}^2 n}{\mathrm{d}y^2} DL\delta y \tag{4}$$

If the screen is placed very close to the flame, then the positions of maximum and minimum intensity can be related to maximum and minimum $\mathrm{d}^2n/\mathrm{d}y^2$ in the flame. At larger distances from the flame, crossing of rays from different parts of the flame complicates the shadow pattern and the relationship does not hold. At sufficiently large L, a discontinuous increase in intensity is observed, and this can be used as a reference point. Weinberg[18] reports that the temperature at this point of maximum deflection is 3/2 times the ambient temperature in air.

In the present investigation, shadow photography was used as the visualization technique. However, other visualization techniques may be utilized to obtain comparable information, which may then be used to infer information regarding scalar and perhaps vector property fields. The ability to resolve vector information quantitatively from changes in the refractive index gradient requires certain assumptions, as discussed by Herman et al.,[19] which best serve simple flows. In certain cases, regions of high gradient may be transported passively by the local flowfield, and thus, the propagation characteristics of such index-or-refraction variations will correlate with the local velocity field, in essence acting as a marker. The present hybrid technique may be used for such purpose in certain flows, but its description herein is limited to the determination of the temperature field as it applies to the flickering diffusion flame investigated.

PIV

The basic relation of displacement divided by time to yield velocity is the fundamental principle of the PIV technique. The displacement information is provided by seeding particles that are suspended in the fluid. Unlike earlier particle tracing methods, however, PIV does not rely on the tracking of individual particles and, hence, offers a higher temporal and spatial resolution of the instantaneous flowfield. Since its introduction in the late 1980s, PIV has grown in its acceptance as a robust velocity measurement technique. Several reviews already offer detailed information on the fundamentals of the technique and its various aspects,[20–22] and hence, only a brief description of the technique as generally applied is outlined.

Tracer particles in the fluid, either naturally or artificially occurring, are illuminated using a thin light sheet, which is pulsed to freeze the particle motion. The Mie scattering from the particles is recorded, typically from a direction normal to the light sheet, at two instances in time using a digital camera. The two sequential digital images are then subsampled at particular areas via a prescribed interrogation window, and a spatial cross correlation is performed using fast Fourier transform (FFT) analysis, as described by Willert and Gharib.[20] The separation time between the light pulses is selected to have particles displace several pixels within the interrogation area

and at most remain common to both images. A high cross-correlation value is observed where many particle images match up with their corresponding spatially shifted partners, and this is considered to represent the best match of particle images between the sequential recordings.

The displacement vector of the cross-correlation peak from the center, that is, origin, of the two-dimensional interrogation window denotes the average distance traveled by the particles within the interrogation area. Accurate estimation of the displacement vector to subpixel resolution is performed by locally fitting the two-dimensional array of correlation values in the vicinity of the peak. The absolute displacement vector is then calculated through a calibration of the magnification factor between the pixel domain of the digital recording device and the physical field of view. Finally, division of the displacement vector, determined for each interrogation area along the entire pixel domain, by the time separation between the two sequential images yields the velocity vector field in the physical area under investigation.

Experimental Setup

Test Configuration

The coannular burner used by Smyth et al.,[23] Shaddix et al.,[24] and Shaddix and Smyth[25] to research time-varying, hydrocarbon diffusion flames with optical imaging methods has been used in the present investigation. The burner consisted of a 1.11-cm-diam fuel tube surrounded by a 10.2-cm-diam air annulus. The air chamber was filled with glass beads followed by several fine mesh screens and a 2.54-cm-thick ceramic honeycomb section with 0.15-cm-square cells to provide a uniform airflow velocity. No beads or screens were used for flow conditioning in the 13.7-cm-long fuel tube. This latter tube was attached to a plenum and extended 0.4 cm above the honeycomb. Ultra chemically pure grade methane was used as fuel. The bulk velocities of the fuel and air were kept constant at 77.8 and 79.0 mm/s, respectively, via calibrated mass flow controllers having an uncertainty of less than 1%.

The flame was acoustically forced by applying a 10.0-Hz, 0.75-V, sinusoidal voltage from a function generator to a loudspeaker attached to the plenum. This generated the moderately flickering flame condition previously investigated by Smyth et al.,[23] Shaddix et al.,[24] and Shaddix and Smyth.[25] In addition, the function generator was synchronized to a delay generator that acted as a variable trigger source for locking in the laser illumination and image recording systems used for shadowgraphy, as shown in the schematic of Fig. 2.

Shadow Image Velocimetry (SIV)

A commercial PIV system was used consisting of a laser illumination source, digital imaging device, and dedicated hardware and software for data analysis. The illumination source was a 200-mJ, double-cavity Nd:Yag laser operating at a wavelength of 532 nm and a pulsation frequency of 15 Hz. To eliminate speckle variations between the laser beams due to the two separate cavities, the laser beam was first expanded and then focused onto a 2-mm-diam glass sphere, which acted as a source. It was then collimated to a diameter of 50 mm. The collimated beam was passed through the flame and imaged onto a screen, located 190 cm from the center of the burner, to generate the shadowgraph. Recording of shadowgraph image pairs was accomplished via an 8-bit double-frame charge-coupled device camera having a resolution of 1008×1018 pixels. This type of camera eliminated image order ambiguity and allowed for the use of cross-correlation methods when determining the velocity vector. Processing of the image maps was done via dedicated hardware for online correlation analysis by means of FFT-based algorithms implemented using programmable electronics. The correlator was housed inside a processor unit, which also contained a memory buffer and camera personality module, as well as a synchronization module for phase locking the laser and camera activation sequences to an external trigger source. Once evaluated, the raw vector map data were passed to a personal computer for visualization and storage. Setting of data acquisition parameters and management of data was accomplished using dedicated software to interact with the programmable processor.

PIV-based image correlation relies on images containing a spotted field generated by the scattering of illuminated particles. However, under normal shadowgraph conditions such a spotted field is not available, and correlation of image pairs yields overwhelmingly invalid vector data. Hence, to apply PIV image processing successfully, a pseudoparticle field was created, as shown in Fig. 3, by inserting a holographic diffuser between the source and the collimating lens (see Fig. 2). The particular holographic diffuser used was made out of a polycarbonate substrate and had a 2-deg diffuser angle. The emanating beam had a top-hat form and provided increased uniformity in the shadow illumination, in addition to generating the pseudo-particle field.

Data Acquisition

The PIV illumination and recording devices were synchronized to coincide in phase with previous measurements and flame

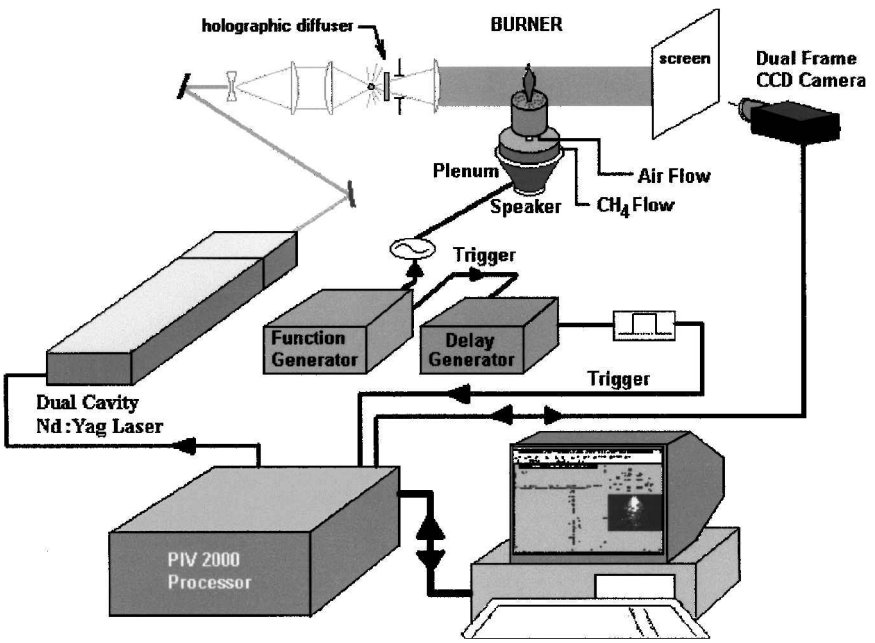

Fig. 2 Schematic of experiment and instrumentation layout.

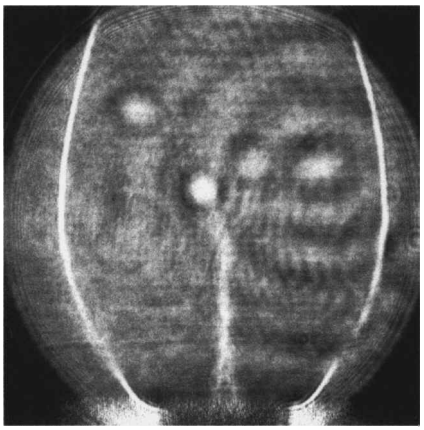

Normal

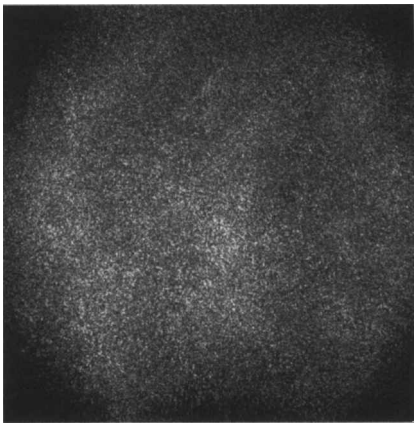

With holographic diffuser in place

Fig. 3 Shadowgraph image of flame at 0% phase.

visualizations reported in Refs. 23–25. Initially shadowgraph images were obtained. While generating these images, the holographic diffuser was removed from the incident light path. Furthermore, the camera was operated in single-frame mode, and only one laser cavity was used to illuminate the flame.

Subsequently, shadow image velocimetry (SIV) data was obtained by installing the holographic diffuser as indicated in Fig. 2 and operating the camera and the laser in the normal PIV sense. The time duration between laser pulse pairs corresponding to one SIV measurement was 1 ms, yielding particle-displacement resolution uncertainties of no more than 1% of the maximum displacement value. Because the pulsation frequency of the PIV lasers was 15 Hz, while flame excitation was at a frequency of 10 Hz, it was necessary to skip two excitation cycles between each SIV recording to phase lock the system. A data acquisition burst was first initiated on an external trigger at the desired phase within a cycle, and then five recordings were performed at a time interval of 200 ms. On receiving the external trigger, the PIV processor synchronized the initiation of the burst measurement within a 100-ns time window. In all, five bursts were recorded at each phase, for a total of 25 SIV realizations per phase.

A field of 900 vectors was determined at each SIV acquisition using a 64-pixel square interrogation area at 50% overlap. A moving-average procedure was used to eliminate invalid vectors before statistical averaging. The spotted field created using the holographic diffuser was quite ideal for generating SIV vector data, with over 99% of the vectors being valid at each recording, and validity did not degrade when a 32-pixel square interrogation area was tested. The uniformity of the pseudoparticle field generated by the holographic diffuser is not dominated by flow dependency, as is a typical particle field in actual PIV experimentation where seeding density nonuniformity is always a concern. Hence, in the present setup, pseudoparticle density was dependent on the placement of the holographic diffuser relative to the spatial filter. This gave a robust way of optimizing the PIV signal to noise in terms of the number of particles correlated within each pair of interrogation areas.

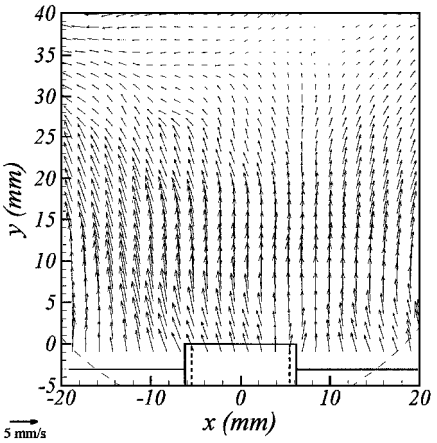

Fig. 4 Average velocity field obtained at the flame-off condition.

A concern was, however, the misalignment between the optical path of the two separate lasers. Because laser illumination for each pulse comes from separate laser cavities, such misalignment will introduce a velocity bias into the results. To minimize this bias, alignment of the laser beam path was performed using the SIV technique to generate a velocity map representing the misalignment and then manually correcting beam overlap so that the velocity field was minimized. Subsequently, the velocity field from a flame-off realization representing beam misalignment was used to correct SIV measurements obtained at the flame-on condition. In the present case, the average value from five realizations at the flame-off condition, shown in Fig. 4, was used.

Results

SIV Characteristics

Results were obtained for the weakly excited flickering flame case investigated in Refs. 23–25. Shadowgraph images obtained using the PIV illumination and recording devices are shown in Fig. 5. The shadow images shown are equally spaced in time within one excitation cycle and coincide in phase with previous measurements and flame visualizations reported by Smyth et al.,[23] Shaddix et al.,[24] and Shaddix and Smyth.[25] The corresponding mean vector maps obtained using the SIV approach are shown in Fig. 6.

A qualitative interpretation of the SIV vector fields was first investigated by comparing them to the corresponding OH-laser-induced fluorescence and soot scattering images reported by Smyth et al.,[23] as shown in Fig. 7. The location of the flame front is marked by the high-intensity band of the hydroxyl radical, whereas the outer high intensity band of the shadowgraph (see Fig. 5) corresponds to the maximum deflection location discussed by Weinberg.[18] This latter high-intensity band is due to the coalescence of light rays through and around the flame. Because the SIV technique yields information on the rate of change of this coalescence, a sign change in the horizontal component of velocity is observed, as indicated in the vector plot of Fig. 7. Contours of the spatial derivatives of the horizontal and vertical velocities, also shown in Fig. 7, reveal interesting topologies. A local minimum of dU/dx corresponds to a location where the coalescence of light rays is observed in the shadowgraph. Such a minimum is also observed just above the burner exit for dV/dy, which corresponds to light ray coalescence due to cold fuel injection during this part of the flickering cycle. Finally, the locus of points where $dU/dx = 0$ while moving radially outward from the inner flame region is coincident with the lean side of the flame front.

Temperature Evaluation

Pitts[26] recently introduced a system for thin-filament pyrometry, which was tested in the acoustically phase-locked flickering laminar methane/air diffusion flame discussed herein. Results were

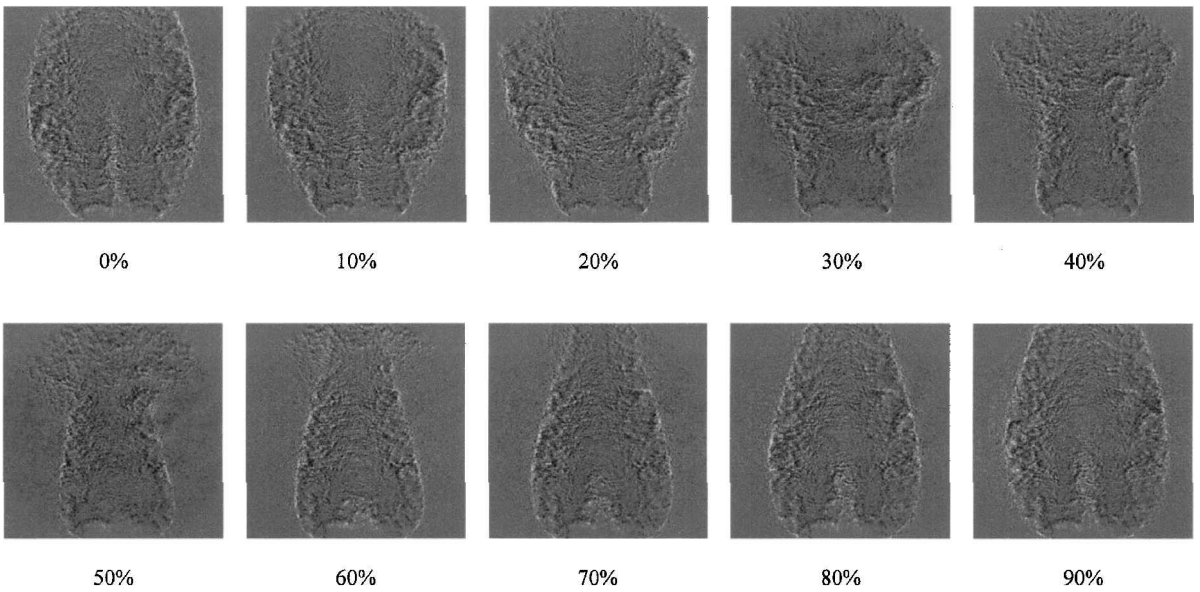

Fig. 5 Background-subtracted shadow images of the weakly perturbed flickering flame near the burner exit; every 1/10-th phase shown, starting with 0% phase at the upper-left-hand corner, with 100 ms total time sequence. (Field of view dimensions for each shadow image are 47.6 mm wide × 48.1 mm high.)

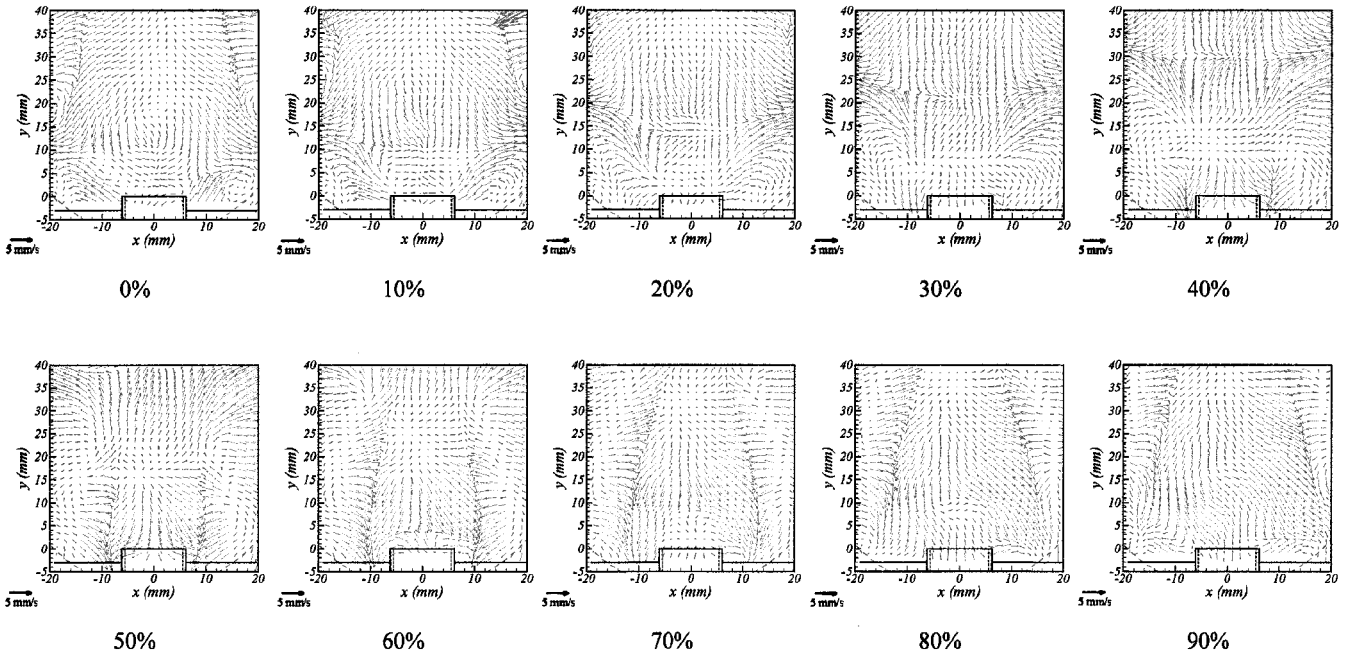

Fig. 6 Resulting vector maps for the weakly perturbed flickering flame at the burner base using shadow image velocimetry; every 1/10-th phase shown, starting with 0% phase at the upper-left-hand corner, for 100 ms total time sequence.

shown for radial profiles of measured filament temperature at several heights above the burner for a phase of 60%. Considering the temperatures along the centerline of the burner only, the data reported by Pitts[26] are shown in Fig. 8. These temperature measurements are helpful toward understanding the present results. In performing the thin-filament pyrometry measurements, Pitts[26] utilized an imaging technique that could not resolve temperatures below 1200 K. Therefore, even though radial measurements were obtained at a location of 5 mm above the burner, in the vicinity of the centerline no temperatures were reported because actual temperatures were below the 1200-K limit of the imaging technique used.

A difficulty that arises with regard to interpreting quantitatively the SIV results in flames is that changes in the shadow are due to index of refraction changes, which in turn are due to temperature and concentration changes. However, if the time separation between laser pulse pairs is short in relation to flame front movement, yet long in relation to chemical reaction times, it can be assumed that changes in the index of refraction are most affected by the temperature field. As mentioned earlier, shadowgraphy produces a pattern that is related to the second spatial derivative of the index of refraction. However, the SIV result yields information on how fast the instantaneous shadowgraph field is changing. Therefore, it follows that the SIV field is proportional to the instantaneous temperature gradient field. This information is two dimensional, as indicated by the SIV results of Fig. 6.

Centerline

Along the centerline of the burner, the horizontal component of the SIV field is approximately zero, as expected from flow symmetry, and the vertical component may be considered for further interpretation. A plot of the vertical component of the SIV field along the burner centerline and for 60% phase is shown in Fig. 8.

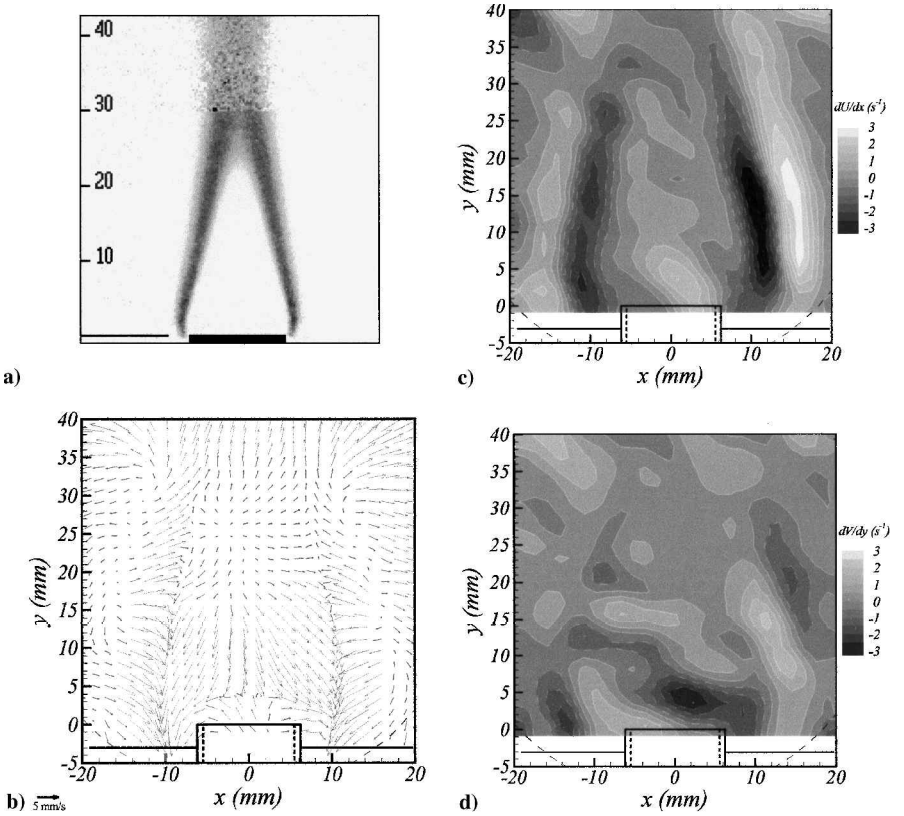

Fig. 7 Results for 60% phase (dashed lines in the contour plots indicate regions of negative value): a) two-dimensional hydroxyl radical fluorescence and soot scattering image as reported by Smyth et al.,[23] b) SIV vector map, c) SIV horizontal velocity spatial derivative, and d) SIV vertical velocity spatial derivative.

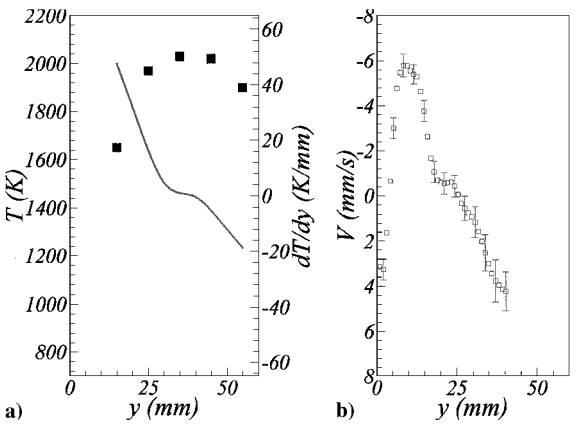

Fig. 8 Results of the 60% phase along the burner centerline: a) filament temperatures (symbols) as reported by Pitts[26] and calculated temperature gradient (line) and b) SIV vertical component result. (Note that the vertical axis is reversed; error bars represent standard deviation of acquisition.)

Note that the scale for the ordinate is reversed to enhance the fact that the SIV vertical component correlates negatively with the temperature gradient calculated from the temperature data of Pitts,[26] also shown in Fig. 8. This verifies that the velocity field obtained using the SIV technique is proportional to the temperature gradient field. The negative correlation comes about from the relationship between the index-of-refraction gradient, that is, temperature gradient, and the ray deflection angle, as indicated in Eq. (2). The relationship between the two, however, is complicated by the three dimensionality of the flame, which affects the results by introducing several biases. First, a negative offset in the y direction of the SIV result, in comparison to the filament temperature curve, is attributed to the absolute angular deflection of light rays at the flame-on condition. Second, the thickness of the flame is not constant along the vertical and horizontal directions. Nonetheless, the trend does follow the temperature gradient curve, which should itself be taken as an estimate because not enough data points were available for its accurate determination.

From the centerline SIV data shown, the actual temperature distribution along this one direction may be obtained by performing an integration of the form

$$T(0, y) = -\int_0^y \kappa_0 \cdot \mathrm{SIV}(0, y) \cdot \mathrm{d}y + T_{\mathrm{ref}}(0, y_0) \qquad (5)$$

where κ_0 is a proportionality constant that depends on the shadowgraph/schliere configuration and T_{ref} $(0, y_0)$ is a reference temperature at $y = y_0$.

A direct determination of κ_0 was not investigated further within the scope of this preliminary reporting of the SIV technique and is left for future work. The integration was, thus, performed using an iterative procedure in which values of κ_0 and T_{ref} $(0, y_0)$ were selected so as to give the filament temperatures at $y = 15$ and 25 mm reported by Pitts,[26] shown in Fig. 8. In addition, a third constant ζ was introduced to correct for the displacement bias between the curves, which serves as an amplifier to the vertical distance variable y. The integration was performed several times to incorporate randomly the error in the mean value of the SIV data shown in Fig. 8. The resulting values were $\kappa_0 = 11.8\ \mathrm{s \cdot K/mm^2} \pm 0.2\ \mathrm{s \cdot K/mm^2}$, $T_{\mathrm{ref}}(0, 0) = 1143\ \mathrm{K} \pm 45\ \mathrm{K}$, and $\zeta = 1.35 \pm 0.35$ at a 95% confidence level. The final temperature along the centerline of the burner for 60% phase is shown in Fig. 9. The shape of the temperature distribution was captured nicely, and temperatures lower than 1200 K were determined for locations of $y < 9$ mm, agreeing with the observation of Pitts.[26] Furthermore, the local minimum at the location $y = 4$ mm coincides with injected fuel during this phase of the flickering cycle, whose temperature would be lower than the surrounding fluid.

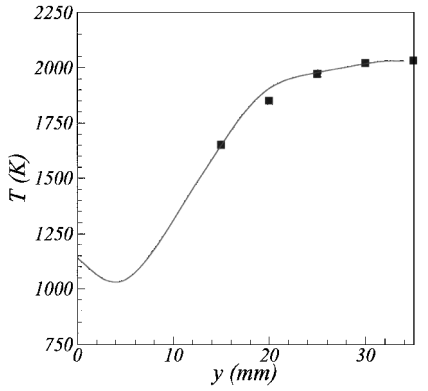

Fig. 9 Temperature distribution along the centerline of the flame: symbols are thin-filament temperatures reported by Pitts[26] and line is temperature calculated from the SIV data following integration.

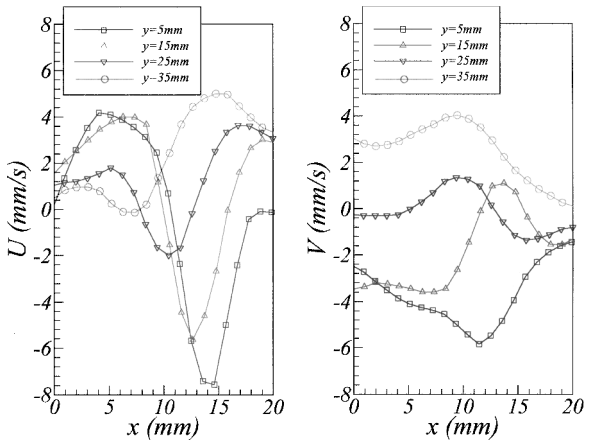

Fig. 10 Profiles of SIV horizontal and vertical components at several elevations above the burner exit.

Whole Field

Distributions of the horizontal and vertical components of SIV velocity at several heights above the burner exit are shown in Fig. 10. Converting these to temperatures requires a similar integration procedure, namely,

$$T(x, y) = \int_0^x \kappa_0[U(x, y) - V(x, y)]\,dx + T(x, 0) \qquad (6)$$

where κ_0 is the same proportionality constant evaluated previously for the centerline temperature distribution. The results from the centerline temperature distribution were used to provide values for $T(x, 0)$. Performing the integration of Eq. (6) on the data of Fig. 10 yields the temperature distributions shown in Fig. 11. In Fig. 11, the radial temperature distributions reported by Pitts[26] are also shown for comparison.

The agreement between the distributions determined from the SIV vector data and those reported by Pitts[26] is good. The trend of the temperature distribution is captured well at every level, as is the tendency of the temperature peak to move closer to the centerline of the flame. Higher values of peak temperature are determined from the SIV data, which is not an unreasonable result because the thin-filament pyrometry data of Pitts[26] were not corrected for convection effects.

Because of the nature of the shadowgraph formulation, the temperature distribution calculated from the SIV data shows increasing temperature distributions past the location of light-ray coalescence. The nature of light-ray deflection in the horizontal direction is different on either side of this boundary, and although the integration

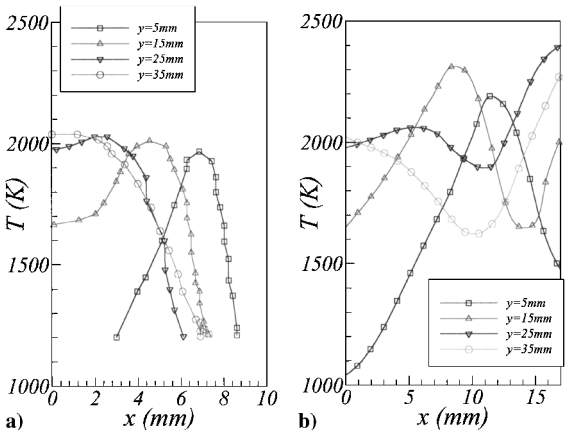

Fig. 11 Temperature distribution results at several levels above the burner exit: a) thin-filament pyrometry results reported by Pitts[26] and b) results from SIV field integration.

works well on the inner region, it needs to be modified for use in the outer region, an objective of future work. Furthermore, the band of light-ray coalescence is largely due to the curved nature of the flame, which tends to amplify light-ray deflections, as discussed by Weinberg.[18] This explains the horizontal location bias that is inherent in the SIV-determined temperature distribution shown in Fig. 11. For the sake of comparison, the horizontal ranges on the plots of Fig. 11 were selected so as to spread the distributions similarly within the plotting area. Proper handling of these shadowgraph-induced biases is the current task at hand.

Conclusions

A novel approach that combines a refractive-index visualization method with the image acquisition and fast postprocessing of the PIV technique was introduced for measuring the velocity of index of refraction gradients in time-varying flows. Depending on the flow under investigation, these gradients may be related to density or temperature gradients. In the present paper, a first application of the technique to a time-varying flame showed that the temperature field may be successfully determined from the velocity information generated by the SIV technique. This was achieved by performing an integration and incorporating primarily two constants, a factor for relating the velocity magnitude to that of the thermal gradient and a reference temperature serving as the constant of integration. A third constant was also needed to correct for light-ray deflection amplification due to the curved nature of the present flame.

The resulting temperature distribution along the centerline, that is, vertical direction, and at several horizontal elevations off the burner base compared well with previous measurements obtained using thin-filament pyrometry. Further interpretation of the two-dimensional velocity information measured by the SIV technique for the time-varying laminar flame is presently under way, which will involve an improved understanding of the proportionality factor and its dependence on the object and shadowgraph configurations.

The simplicity of shadowgraphy is attractive, but because shadowgraphy is an integrated line-of-sight technique, it is not properly suited for complex, three-dimensional flows. A future solution to this would be to replace shadowgraphy with the more sophisticated focusing schlieren technique that has the ability to focus in a fairly thin portion of the optical path.

Acknowledgments

The measurements discussed herein were performed while the author was a National Research Council Postdoctoral Fellow at the National Institute of Standards and Technology (NIST). The support of William Pitts during the author's stay at the Building and Fire Research Laboratory of NIST is most appreciated.

References

[1]Weinberg, F. J., *Optics of Flames*, Butterworths, London, 1963, pp. 116–235.

[2]Weinberg, F. J., and Wong, W.-Y., "Optical Studies in Fire Research," *16th Symposium (International) on Combustion*, Combustion Inst., Pittsburgh, PA, 1977, p. 799.

[3]Weinberg, F. J., "Optical Methods in Combustion Research," *International Symposium on Flow Visualization*, Hemisphere, Washington, DC, 1982, pp. 3–14.

[4]El Wakel, M. M., "Interferometry in Flames," *Combustion Measurements*, edited by R. Goulard, Academic Press, New York, 1976, pp. 225–244.

[5]Bachalo, W. D., and Houser, M. J., "Optical Interferometry in Fluid Dynamics Research," *Optical Engineering*, Vol. 24, May–June 1985, pp. 455–461.

[6]Sankar, S. V., Buermann, D. H., and Bachalo, W. D., "Application of Rainbow Thermometry to the Study of Fuel Droplet Heat-Up and Evaporation Characteristics," *Journal of Engineering for Gas Turbines and Power*, Vol. 119, No. 3, 1997, pp. 573–584.

[7]Mercer, C. R., and Creath, K., "Liquid Crystal Point Diffraction Interferometer for Wavefront Measurements," *Applied Optics*, Vol. 35, No. 10, 1996, pp. 1633–1642.

[8]Goldmeer, J. S., Urban, D. L., and Yuan, Z.-G., "Interferometer Development for Study of Interactions Between Flames on Parallel Solid Surfaces," *Fifth International Microgravity Combustion Workshop*, NASA John H. Glenn Research Center at Lewis Field, May 1999, pp. 501–504.

[9]Kafri, O., "Noncoherent Method for Mapping Phase Objects," *Optics Letters*, Vol. 5, Dec. 1980, pp. 555–557.

[10]Stricker, J., and Kafri, O., "Moiré Deflectometry, a New Method for Density Gradient Measurements in Compressible Flows," *AIAA Journal*, Vol. 20, No. 3, 1982, p. 820.

[11]Keren, E., Bar-Ziv, E., Glatt, I., and Kafri, O., "Measurements of Temperature Distribution of Flames by Moiré Deflectometry," *Applied Optics*, Vol. 20, Dec. 1981, pp. 4263–4266.

[12]Howes, W. J., "Rainbow Schlieren," NASA TP 2166, May 1983.

[13]Howes, W. J., "Rainbow Schlieren and Its Applications," *Applied Optics*, Vol. 23, July 1984, pp. 2449–2460.

[14]Greenberg, P. S., Klimek, R. B., and Buchele, D. R., "Quantitative Rainbow Schlieren Deflectometry," NASA TM-111231, July 1995.

[15]Kantrowitz, A., and Trimpi, R., "A Sharp Focusing Schlieren System," *Journal of the Royal Aeronautical Society*, Vol. 17, No. 5, 1950, p. 311.

[16]Burton, R. A., "A Modified Schlieren Apparatus for Large Areas of Field," *Journal of the Optical Society of America*, Vol. 39, No. 2, 1949, p. 907.

[17]Weistein, L. M., "Large-Field High-Brightness Focusing Schlieren System," *AIAA Journal*, Vol. 31, No. 7, 1993, pp. 1250–1255.

[18]Weinberg, F. J., "The Shadowgraph of a Flat Flame," *Proceedings of the Royal Society of London, Series A: Mathematical and Physical Sciences*, Vol. 235, 1956, pp. 510–517.

[19]Herman, C., Kang, E., and Wetzel, M., "Expanding the Applications of Holographic Interferometry to the Quantitative Visualization of Complex, Oscillatory Thermofluid Processes," *Experiments in Fluids*, Vol. 24, No. 5/6, 1998, pp. 431–446.

[20]Willert, C. E., and Gharib, M., "Digital Particle Image Velocimetry," *Experiments in Fluids*, Vol. 10, No. 4, 1991, pp. 181–193.

[21]Adrian, R. J., "Particle Image Techniques for Experimental Fluid Mechanics," *Annual Review of Fluid Mechanics*, Vol. 23, 1991, pp. 261–304.

[22]Lourenco, L. M., Krothapalli, A., and Smith, C. A., "Particle Image Velocimetry," *Advances in Fluid Mechanics Measurements*, Springer-Verlag, Berlin, 1989, p. 127.

[23]Smyth, K. C., Harrington, J. E., Johnson, E. L., and Pitts, W. M., "Greatly Enhanced Soot Scattering in Flickering CH_4/Air Diffusion Flames," *Combustion and Flame*, Vol. 95, No. 1/2, 1993, pp. 229–239.

[24]Shaddix, C. R., Harrington, J. E., and Smyth, K. C., "Quantitative Measurements of Enhanced Soot Production in a Flickering Methane/Air Diffusion Flame," *Combustion and Flame*, Vol. 99, No. 3/4, 1994, pp. 723–732.

[25]Shaddix, C. R., and Smyth, K. C., "Laser-Induced Incandescence Measurements of Soot Production in Steady and Flickering Methane, Propane, and Ethylene Diffusion Flames," *Combustion and Flame*, Vol. 107, No. 4, 1996, pp. 418–452.

[26]Pitts, W. M., "Thin-Filament Pyrometry in Flickering Laminar Diffusion Flames," *Twenty-Sixth Symposium (International) on Combustion*, Combustion Inst., Pittsburgh, PA, 1996, pp. 1171–1179.